Opposite current states in concentric ring exciton-polariton condensates

Vladimir Lukoshkin,[1,2] Vladimir Kalevich,[1,2] Evgeny Sedov,[2,3,4,*] and Alexey Kavokin[2,4,5]

[1] *Ioffe Institute, Russian Academy of Sciences, 26 Politekhnicheskaya, St. Petersburg 194021, Russia*
[2] *Spin Optics Laboratory, St. Petersburg State University, Ulyanovskaya 1, St. Petersburg 198504, Russia*
[3] *Stoletov Vladimir State University, 87 Gorky str., Vladimir 600000, Russia*
[4] *School of Science, Westlake University, 600 Dunyu Road, Hangzhou, Zhejiang Province 310030, China*
[5] *Moscow Institute of Physics and Technology, Institutskiy per., 9, Dolgoprudnyi, Moscow Region 141701, Russia*

(Received 22 August 2024; accepted 22 October 2024; published 12 November 2024)

This work explores the excitation of a two-mode exciton-polariton condensate within a ring-shaped trap, with each mode manifesting as a distinct eigenstate characterized by oppositely directed azimuthal polariton currents. The coexistence of these condensate states is facilitated by a positive gain-loss balance for both states, sustained by external noncoherent laser pumping. We utilize interferometric methods to investigate these states. Spherical wave interferometry visualizes the azimuthal polariton currents and elucidates the spatial phase properties of the condensates. Plane-wave interferometry with a self-delayed replica of the condensate's photoluminescence provides a highly sensitive approach for estimating the energy splitting between the states. The experimental observations are validated by numerical simulations. The study emphasizes the potential of these condensates to form the basis for flux polariton qubits, leveraging the superposition of current states within an annular optical trap.

DOI: 10.1103/PhysRevApplied.22.054031

I. INTRODUCTION

The strong coupling of light photons with excitons within semiconductor quantum wells in specially designed optical microcavities [1] leads to the emergence of hybrid quasiparticle exciton polaritons. These quasiparticles combine the properties of both light and matter, which makes them pivotal in the exploration of complex light-matter interactions, including various quantum phenomena. Namely, being bosons, polaritons can reach a state of coherence that mirrors the properties seen in Bose-Einstein condensates [2]. This state is characterized by a macroscopic occupation of a single quantum state by many bosons, which is an impressive feat given the inherently nonequilibrium nature of polariton systems due to their finite lifetimes. These polariton condensates exist only under nonequilibrium conditions, maintained by a steady supply of energy from external sources.

The engineering of potential landscapes in these microcavities allows for the manipulation of exciton-polariton flows, creating intricate patterns of internal fluxes. This capability is crucial for probing their superfluidlike properties and exploring their applications in areas such as quantum fluids and optical vortex manipulation [3–6]. Notably, the annular and other complex trap potential geometries facilitate the study of discrete orbital angular-momentum (OAM) states, essential for understanding the quantum behaviors of macroscopic objects within these condensates [7–9].

Research in this field has increasingly focused on the intentional creation and control of polariton vortices, which represent the most striking manifestations of OAM within polariton condensates. These vortices can form spontaneously [10–12] and can be engineered with predefined OAM through various methods, including resonant excitation and imprinting of OAM [7,13], mechanical rotation of traps [14–18], or even the less understood technique of directly transferring OAM from a nonresonant optical pump [19]. Such techniques enable precise control over the direction and distribution of polariton flow, opening up possibilities for targeted manipulations in quantum information processing and beyond [20–24]. Furthermore, the development of optically induced traps and barriers has provided a flexible approach to localize and control polaritons [25,26]. Optically induced incoherent exciton reservoirs serve as potential barriers that, depending on their configuration, either complement existing traps or independently shape the geometry of the condensate, thus influencing its dynamic state properties. This approach has been successful in forming polariton condensates in various shapes, such as rings or multiple spots, which are instrumental in studying azimuthal polariton currents and their modal characteristics [27–36].

The spatial configuration of traps for polaritons plays a critical role in the phase relationships and coherence properties of the condensates. Experiments and simulations

*Contact author: evgeny_sedov@mail.ru

have shown that polariton condensates, when placed in overlapping or closely situated traps, exhibit complex interactions, such as Josephson oscillations and coupled spin-orbital dynamics [37–39]. Beyond these typical Josephson junctions, long Josephson junctions introduce an extension to the dynamics of polariton condensates [40,41]. These extended junctions support the formation of Josephson vortices, localized disruptions in the polariton flows. In ring-shaped or annular geometries, these long Josephson junctions are particularly effective in facilitating structured polariton currents. They possess a distinct ability to enable condensates with concentric circular currents, each potentially possessing different winding numbers. This configuration allows for an intricate phase landscape across the rings, where Josephson vortices help to balance phase mismatches between adjacent rings, thereby stabilizing the overall condensate structure.

The creation of polariton condensates in the form of concentric rings has become a routine experimental achievement. Forming such structures does not always require complex profiling of the trapping potential, unlike what is needed for Josephson-like configurations. In a series of our studies [31,32,42], we have extensively explored the concentric ring condensates, ranging from noncurrent to current-carrying states. These investigations have successfully demonstrated both stationary current states and oscillating vorticity regimes, where the direction of the current varies over time. In concentric ring condensates, however, achieving opposing currents simultaneously across the rings is fundamentally constrained by the unified wave function, which must maintain a single-valued, continuous phase.

Nevertheless, due to the inherently nonequilibrium nature of polariton condensates, which necessitates external (optical) pumping to compensate for the inevitable losses primarily due to the finite quality factor of microcavity structures, the simple ring geometry of traps offers the potential to excite current states with different, and particularly opposite, winding numbers, simultaneously. In polariton experiments, when polaritons are placed within a trapping potential, they form a condensate in an eigenstate of this trap. However, this eigenstate does not necessarily have to be the ground state of the trap. Rather, the condensate forms in any state where the balance between pumping and losses becomes positive. This outcome is largely determined by the extent of overlap between the condensate's wave function and the incoherent exciton reservoir, excited by the laser pump beam, that acts as its feeder. The balance is primarily influenced by factors such as the size of the trap and the power of the laser pump [31,43]. It is noteworthy that under certain experimental conditions, the gain-loss balance can be positive for several states of the trap simultaneously. In such instances, the experiment may result in the formation of a polariton state comprising multiple modes that differ in energy, spatial structure, and dynamic characteristics [44].

In this paper, we discuss the experimental excitation of two-mode exciton-polariton condensates within a ring-shaped trap using nonresonant optical pumping, where the excited modes exhibit currents flowing in opposite directions. To characterize these states, we employ interferometric techniques, providing a clear depiction of their dynamic behaviors and energetic disparities. To differentiate the energy levels of the excited modes, we employ plane-wave interferometry. We judge the energy differences between the modes by observing the relative displacement of the interferometry fringes in different spatial regions of the observation area, which correspond to the predominant concentration of a particular mode. We confirm the presence of vortices through a reliable approach previously proposed by us [28], which involves observing the interference with a reference spherical wave. The presence of polariton currents in opposite directions is indicated by interference spiral fringes that twist in opposite directions in the respective radial regions of the polariton condensate state. We elucidate the structure of the observed modes and validate our experimental observations through numerical simulations based on a two-mode extension of the generalized Gross-Pitaevskii equation.

II. SAMPLE AND SETUP

We treat nonresonant laser excitation of exciton-polariton condensates in a cylindrical micropillar. The micropillar of a diameter of 30 μm is etched from a planar $5\lambda/2$ (Al, Ga)As distributed Bragg reflector microcavity with a quality factor of about 1.6×10^4. To enhance exciton-photon coupling, four sets of three GaAs quantum wells 10 nm in thickness were positioned at the electric field antinodes of the cavity [45]. The microcavity's wedge design allowed for scanning across the sample to adjust the exciton-photon detuning energy in the range $-(0.5 \div 3.5)$ meV. The sample is placed at a helium-flow cryostat at a temperature of $T = 4$ K.

Our experimental methodology involves three types of measurements to analyze properties of the condensates. The first measurement type is the direct detection of photoluminescence (PL) of the condensate, as it provides insight into the spatial distribution of its density. The second involves detecting the interference of PL of the condensate with a delayed version of itself. This measurement enables us to probe the coherence properties of the polariton condensate across the sample. The third measurement type involves the interference of PL with a coherent reference spherical wave, allowing for a detailed examination of the phase distribution across the condensate.

To facilitate these investigations, we employ a Mach-Zehnder interferometer-based experimental setup initially devised in Ref. [28], which has been specifically adapted

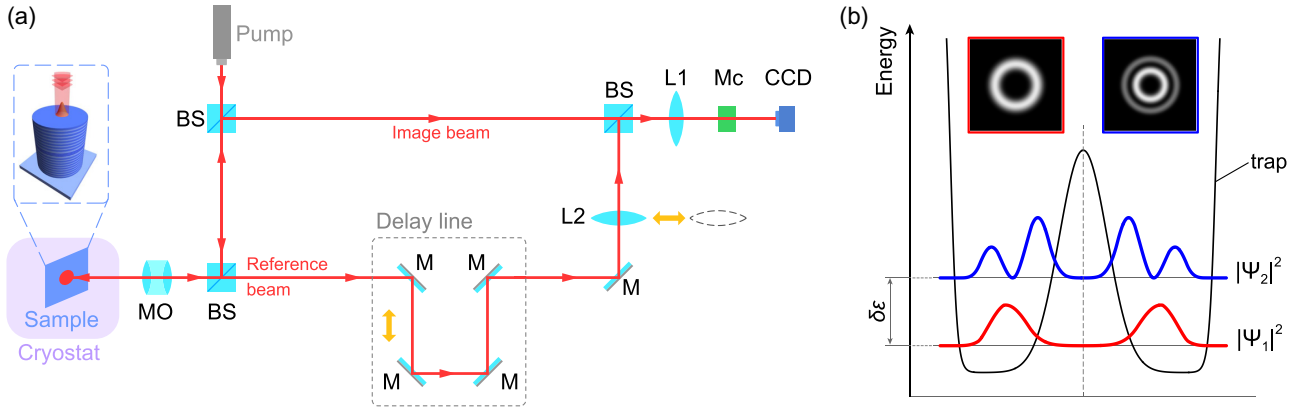

FIG. 1. (a) Schematic of the experimental setup for interferometry measurements. The following abbreviations are used in the figure: beam splitter (BS), microscope objective (MO), mirror (M), lens (L), monochromator (Mc). The horizontal yellow double-sided arrow indicates that lens L2 can be removed for the plane-wave interferometry. The vertical yellow double-sided arrow shows that the length of the delay line can be adjusted to change the phase difference between the image beam and the reference beam. The inset on the left schematically depicts laser excitation of a cylindrical micropillar. (b) Schematic of the splitting of eigenmodes with different radial quantum numbers in a trap. The trap is formed by the stationary potential of the cylindrical micropillar (outer edge) and by the exciton reservoir within the pump spot near the center of the micropillar (central peak). The insets on the top show density plots of the condensate modes Ψ_1 and Ψ_2.

to support the diverse measurements outlined above. The scheme of our setup is shown in Fig. 1(a).

For exciting exciton-polariton condensates, we use a cw Ti:sapphire laser with the radiation energy tuned to a local minimum of the stopband of the upper distributed Bragg reflector, approximately 110 meV above the bottom of the lower polariton branch. The laser beam was focused into a 2-μm spot by a microscope objective (MO) with a numerical aperture of 0.42, which was also used to collect PL emitted by the condensate. After passing through the MO, the PL beam reaches a beam splitter (BS) where it is divided into two paths. The image (upper) beam in Fig. 1(a), after passing through lens L1 with a focal length of $F = 700$ mm, generates an enlarged real image of the condensate at the entrance slit of a 50-cm monochromator (Mc). The lower beam serves as the reference beam. To reveal the phase properties of the condensate, it is transformed into a spherical wave by lens L2 ($F = 100$ mm). For plane-wave interferometry, L2 should be removed from the optical setup. The reference arm is equipped with a delay line that enables precise adjustment of the phase shift by varying the path length. The superimposed image and reference beams (or the image beam alone when the reference beam is blocked for direct PL measurements) are captured by a cooled CCD camera at the monochromator's output.

III. EXPERIMENTAL RESULTS

In our experiment, polariton condensates are excited within a cylindrical micropillar using a spatially localized nonresonant continuous-wave laser beam near the center of the micropillar, see schematic in the inset in Fig. 1(a). In the nonresonant pumping regime, the replenishment of the coherent polariton condensate state occurs indirectly. Initially, the nonresonant pump excites an exciton reservoir, which comprises a cloud of incoherent, high-energy excitonic polaritons primarily localized under and in the immediate vicinity of the pumping spot. The lower-energy polariton condensate is subsequently populated through stimulated scattering from the reservoir. Due to the repulsive interactions among polaritons, the reservoir also serves an additional role as a barrier, contributing to the formation of an effective trapping potential. The resulting potential, formed by the stationary potential of the micropillar and the repulsive barrier created by the reservoir, assumes a ringlike shape. The radial cross section of this trap is schematically depicted by the black curve in Fig. 1(b).

Our goal was to excite current states in ring-shaped polariton condensates, characterized by a nonzero winding number, which is a topological property of the condensate wave function indicating the number of complete phase rotations of the wave function around the ring. The winding number serves as a measure of the vorticity of the condensate state. To achieve our goal, we slightly shifted the pumping spot away from the center of the micropillar. This displacement, combined with the inherent nonuniformity of the polariton landscape in the sample, imparted a chiral characteristic to the system, facilitating the excitation of internal polariton currents within the condensate. This approach has proven to be highly effective for such purposes in our previous research [28–34].

At the pumping power P exceeding the condensation threshold power P_{th} as $P \approx 1.5P_{\text{th}}$, a condensate state consisting of a pair of concentric rings is formed. The detected

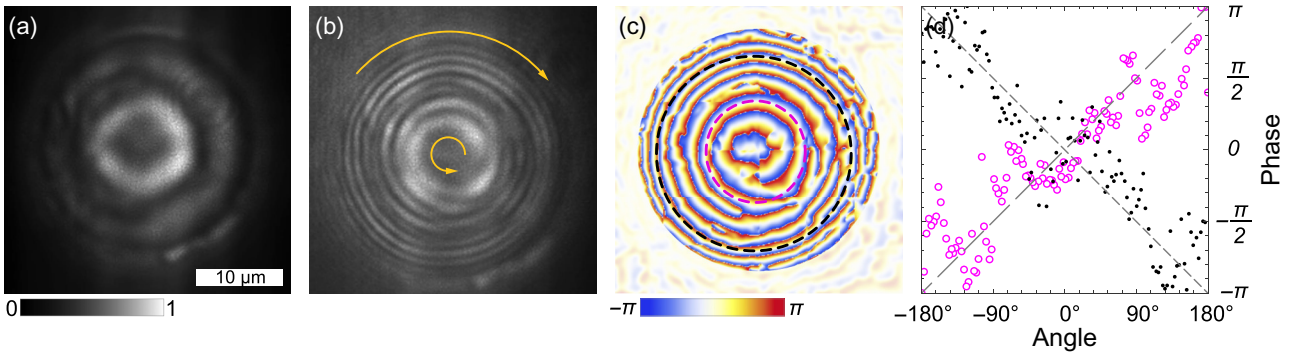

FIG. 2. Observation of the concentric ring polariton condensate with opposite polariton currents. (a) Real-space image of PL of the condensate, (b) the interferometry image obtained from the interference of PL of the condensate and the spherical reference wave, (c) the phase of the condensate relative to the phase of the reference spherical wave extracted from (b) and (d) the phase variation around the closed trajectories indicated by magenta (inner) and black (outer) dashed circles in (c). Yellow arrows in (b) indicate directions of spirals in the inner and outer regions of the interferogram. Dashed lines in (d) are guides for the eye indicating linear variation of the phase. The coordinate origin 0° was chosen arbitrary to minimise the number of breaks of the dependence of the phase on the azimuthal angle. The nonphysical area outside the pillar is shaded in (c).

spatial distribution of PL, that reveals the shape of the condensate, is shown in Fig. 2(a). Qualitatively, this PL distribution is similar to those described in our previous works [31,32,42]. The key difference is observed in the interferogram of the condensate's PL with a reference spherical wave, which provides insights into the phase component of the polariton state, as seen in Fig. 2(b). The distinct interference pattern clearly demonstrates the coherence of the observed state, an inherent characteristic of the polariton condensate. Notably, the interference fringes exhibit a spiral shape, indicative of the presence of azimuthal polariton currents. However, the direction of the spirals in the areas of the inner and outer rings is opposite in the observed state. The distribution of the phase of the state within the micropillar plane relative to the phase of the reference spherical wave, extracted from the interferogram, is presented in Fig. 2(c). Figure 2(d) displays the phase variation in the azimuthal direction along the closed trajectories within different radial regions of the polariton state, which are denoted by the black and magenta rings in Fig. 2(c). The nearly linear increase (magenta) and decrease (black) of the phase with the azimuthal angle along the inner and outer contours, respectively, confirm the presence of polariton currents in opposite directions in the observed state.

As previously mentioned, the combination of concentric rings with oppositely directed polariton currents is characteristic of systems with a ring trap and a long annular Josephson junction [40,41]. In scenarios where a long barrier exists but without local Josephson vortices, a mismatch of winding numbers between the inner and outer areas of the condensates could also be explained by a significant deformation of the trap's shape, enough to consider it elliptical [46]. However, we dismiss both scenarios in our case, as our system lacks any circular barrier capable of providing the necessary radial separation of the condensate. Additionally, the geometry of our trap is undoubtedly closer to circular, with an ellipticity not exceeding a few percent, ruling out significant shape distortion as a contributing factor.

To explain the observed effect, we hypothesize that our observations do not involve a single-polariton condensate but rather a pair of condensate states. These states represent different eigenstates of the ring trap, split in energy and characterized by their own distinct winding number. To validate this hypothesis, we opted for plane-wave interferometry instead of standard frequency spectrometry due to its significantly higher sensitivity. We detected a series of interferograms of the condensate's PL against itself at various phase delays introduced using a delay line, see Figs. 3(a)–3(c). Additionally, a slight angle was introduced between the image and reference beams to ensure the formation of a plane wave within the microcavity plane. The obtained interference fringes are typical for a plane-wave interferometry. The results show that the relative positions of the interference fringes vary across different radial areas of the condensate at different delays. For instance, Fig. 3(b) displays fringes aligned continuously along the chords of the ring trap. In contrast, Figs. 3(a) and 3(c) exhibit a mutual shift of the interference fringes by half a period. We attribute this behavior to different phase increments of the contributing pair of polariton states due to their energy differences. The phase difference of 2π between Figs. 3(a) and 3(c) corresponds to a delay of about 6.7 ps between the beams in the different arms of the interferometer resulting from an optical path-length difference in the delay line of approximately 2 mm. This allows us to estimate the energy splitting of the contributing states at roughly 0.6 meV.

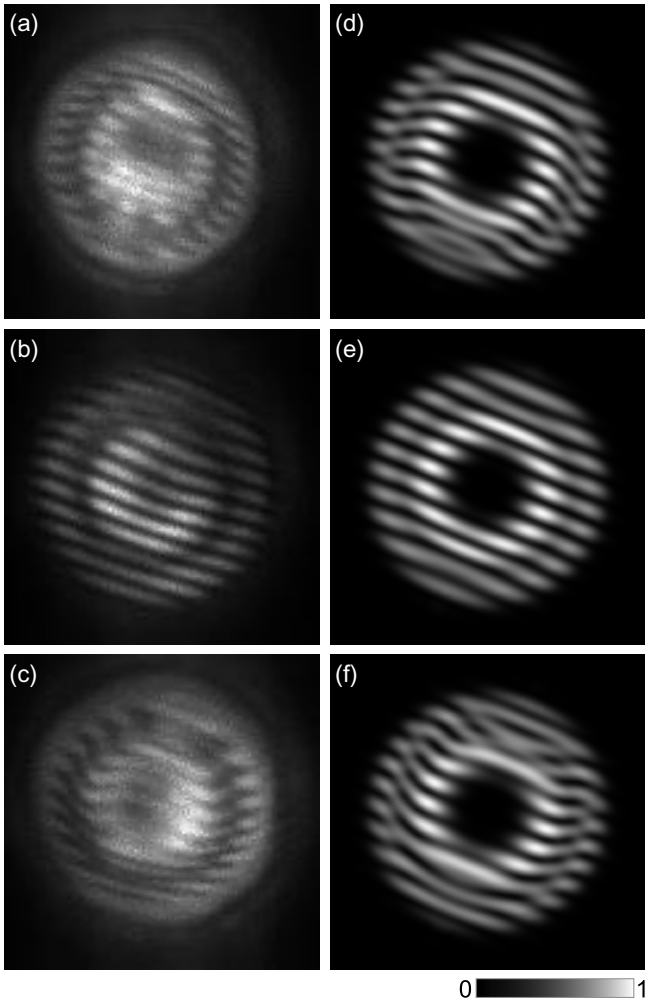

FIG. 3. Experimental observations (a)–(c) and numerical simulations (d)–(f) of interferograms obtained from the interference of the photoluminescence of the concentric ring condensate with a delayed version of itself. The image and reference beams are slightly tilted relative to each other, resulting in interference fringes typical for plane-wave interference. The upper, middle, and lower panels differ by the amount of the introduced delay between the arms of the interferometer. In the experiment, the delay of about 6.7 ps between (a) and (c) corresponds to a change in the reference arm length of the interferometer by approximately 2 mm.

IV. SIMULATIONS

To validate our observations, we complement our experiment with numerical simulations of the behavior of the two-mode polariton condensate in an annular trap under the nonresonant pumping. We describe the evolution of two modes of the polariton condensate characterized by the wave functions $\Psi_j(t,\mathbf{r})$ with $j=1,2$ by the generalized Gross-Pitaevskii equations:

$$i\hbar\partial_t\Psi_j(t,\mathbf{r}) = (1-i\eta)\left[-\frac{\hbar^2}{2M}\nabla^2 + \frac{(-1)^j}{2}\delta\varepsilon + U_j(t,\mathbf{r})\right] \times \Psi_j(t,\mathbf{r}) + \frac{i\hbar}{2}\left[R_j n_{\mathrm{R}}(t,\mathbf{r}) - \gamma_j\right]\Psi_j(t,\mathbf{r}), \tag{1}$$

coupled to the rate equation for the density of the exciton reservoir $n_{\mathrm{R}}(t,\mathbf{r})$:

$$\partial_t n_{\mathrm{R}}(t,\mathbf{r}) = P(\mathbf{r}) - \left[\gamma_{\mathrm{R}} + \sum_{j=1}^{2} R_j|\Psi_j(t,\mathbf{r})|^2\right] n_{\mathrm{R}}(t,\mathbf{r}). \tag{2}$$

In Eq. (1), M is the effective mass of polaritons in the microcavity plane, η characterizes energy relaxation. $\delta\varepsilon$ is the splitting in energies of the treated polariton modes. $U_j(t,\mathbf{r})$ is the effective potential for polaritons composed of several components, as the following:

$$U_j(t,\mathbf{r}) = V(r) + \alpha|\Psi_j(t,\mathbf{r})|^2 + \alpha_{12}|\Psi_{3-j}(t,\mathbf{r})|^2 + \alpha_{\mathrm{R}} n_{\mathrm{R}}(t,\mathbf{r}) + G\bar{P}(\mathbf{r}). \tag{3}$$

The first component $V(r) = V_{\mathrm{R}}(r) + iV_{\mathrm{I}}(r)$ is the stationary potential of the pillar, which is complex in the general case. The real part is taken as $V_{\mathrm{R}}(r) = V_0\{\tanh[a(r-d/2)]+1\}/2$, where V_0 and d are the height of the potential and the diameter of the pillar, a is a fitting parameter responsible for the steepness of the walls of the potential. The imaginary part of the potential is responsible for damping due to etching of the microcavity [47,48]. It repeats the form of the real part with the parameters $V_0 \to V_0'$, $d \to d'$ and $a \to a'$.

The second, third, and fourth components in Eq. (3) characterize blueshift of the condensate energy due to polariton-polariton interactions within the modes and between the modes, and polariton-exciton interactions, respectively, with α, α_{12}, and α_{R} being the corresponding interaction constants. The last component in Eq. (3) characterizes an additional pump-induced blueshift, which can be attributed to the reservoir of dark (optically inactive) excitons, inevitably arising under the pump spot due to, e.g., pseudospin relaxation processes and the acquisition of wave vectors beyond the light cone [49,50]. G is the interaction constant. Nonconservative processes in the system include gain and loss. R_j is the stimulated scattering rate from the reservoir to the condensate mode j; γ_j and γ_{R} are the decay rates of polaritons and reservoir excitons.

The reservoir is excited by the nonresonant optical pump $P(\mathbf{r}) \propto \exp(-r/w)^2$, where w is the width of the pump spot. To determine the shape of the mentioned above dark reservoir, we take $\bar{P}(\mathbf{r})$ of the same form as $P(\mathbf{r})$, but with different width, $\bar{w} < w$, to take into account a finite diffusion of bright excitons away from the pump spot.

In our analysis, we treat the ground, $\Psi_1(t,\mathbf{r})$, and first excited, $\Psi_2(t,\mathbf{r})$, radial states of the ring trap, respectively,

characterized by the polariton density distribution forming single and double rings. The radial cross sections of these states are schematically depicted in Fig. 1(b). In the simulations, using the system parameters specified in Ref. [51], we solve the dynamic Eqs. (1)–(2) until a steady state is reached. Since in our modeling we do not aim to reproduce the mechanisms underlying the formation of the pair of polariton current states, but rather focus on their coexistence in the steady-state regime, we introduce the vortices in our simulations by setting initial conditions with seeds that have the appropriate vorticities. The pump power serves as a control parameter for exciting specific polariton states. By adjusting the pump power, it is possible to vary the relative intensity of the excited polariton states, thereby influencing the visibility of the corresponding interference fringes on the resulting interferogram.

The spatial distribution of density and phase for the two modes of the polariton condensate, obtained from simulations, is presented in Fig. 4. As illustrated, the polariton states support polariton vortices in opposite directions. The winding numbers are calculated as $m_j = (2\pi)^{-1} \oint_{\mathcal{C}} \nabla \arg[\Psi_j(\mathbf{r})] d\mathbf{r}$, where $\arg[\Psi_j(\mathbf{r})]$ is the phase of the condensate state j, and $\mathcal{C}$ is a closed path that encircles the vortex core at the center of the micropillar. For the states in Fig. 4 they are found as $m_{1,2} = \mp 1$. The vector fields of the current density $\mathbf{J}_j = \mathrm{Im}[\Psi_j(\mathbf{r})^* \nabla \Psi_j(\mathbf{r})]$, which visually illustrate the polariton flows within each condensate mode in the steady state, are depicted as blue droplets on (a) and (c).

In Figs. 5(a) and 5(b), we numerically qualitatively reproduce the density distribution of polaritons in the emerging condensate states and the interferometry image obtained when interfering with a spherical reference wave, cf. Figs. 2(a) and 2(b). To enhance similarity with the experimental observations, we introduced a minor lateral shift of the reference beam in the micropillar plane. The phase distribution and azimuthal phase variation extracted from Fig. 5(b) are presented in Figs. 5(c) and 5(d), respectively.

In the simulations, we selected a pump power such that the population of the ground state was approximately 0.85 times that of the first excited state. Under these conditions, as evident in Fig. 5(a), despite partial overlap of the emerging polariton states, the resulting density distribution distinctly features a pair of rings. It is apparent that the state $\Psi_2(\mathbf{r})$ prevails within the inner observational area, while the state $\Psi_1(\mathbf{r})$ prevails within the outer area. Based on this, it is reasonable to expect that in interferometric experiments, the interference patterns in the corresponding radial areas of the condensates will predominantly reflect the prevailing polariton mode. This is corroborated by Figs. 5(b)–5(d).

Our simulations also qualitatively confirm that the experiment indeed captures a doublet of polariton states in the trap. The simulated interference of polariton states in plane waves at various phase delays, shown in Figs. 3(d)–3(f), effectively reproduces the experimental observations.

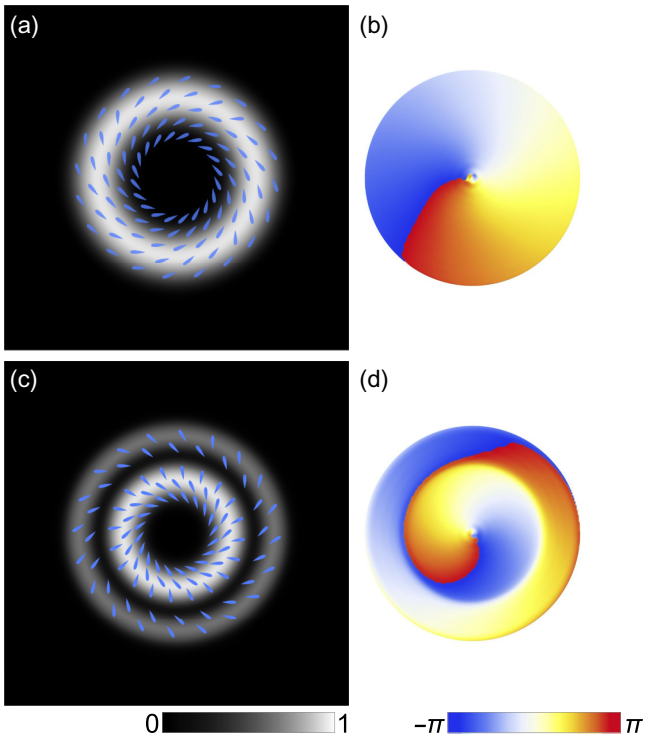

FIG. 4. Simulated steady-state spatial distribution of density (left) and phase (right) of the polariton states $\Psi_1(\mathbf{r})$ (a),(b) and $\Psi_2(\mathbf{r})$ (c),(d), that contribute to the observations in Fig. 5. Blue drops in (a),(c) represent the vector field of the polariton current density $\mathbf{J}_{1,2}$ in the corresponding state.

V. DISCUSSION AND CONCLUSIONS

In this study, we have demonstrated the excitation of a pair of annular condensate states within a ring trap, each characterized by topological charges of opposite signs. Through PL measurements, we observed that the resulting intensity distribution forms a double-ring pattern with some azimuthal modulation, consistent with our earlier observations [31,32,42]. Interferometric measurements using a spherical reference wave unveiled the presence of azimuthal polariton currents flowing in opposite directions across different radial zones of the observation area. Plane-wave interferometry of the condensate's PL, delayed in time relative to itself, substantiated our hypothesis that the observed pair of currents are characteristic of two distinct eigenstates of the ring trap. These states coexist under external optical pumping and are split in energy. We have replicated the experimental observations through numerical simulations, simultaneously uncovering the internal structure of the contributing condensate states.

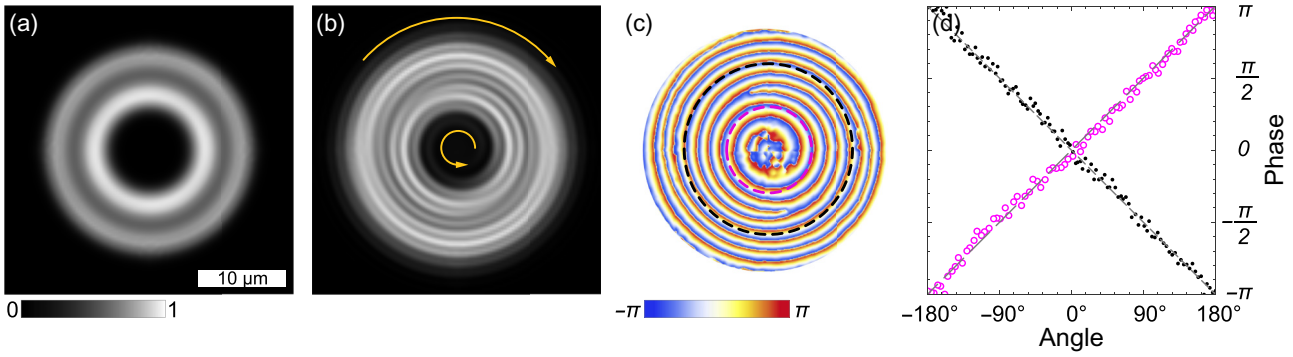

FIG. 5. Simulation of the interferometry of the concentric ring polariton condensates with opposite polariton currents. The meaning of the panels is the same as in Fig. 2.

In both types of interferometric experiments, once the interferograms appeared, they remained unchanged for an extended period until the pumping was turned off. Despite involving two polariton states with different energies, the experimental setup in both cases allowed for the observation of distinctly visible interference patterns. In the first experiment, the reference spherical wave was generated by focusing the luminescence signal from a small area of the condensate, located in the outer region of the observation zone, through a converging lens positioned far beyond its focal length. This setup transformed the planar wave front of the incident radiation into a spherical wave front, converging outside the focal length of the lens. Since both states were present in the selected area, the reference beam effectively comprised two spherical waves with frequencies corresponding to those of the polariton states. Consequently, each state interfered with its coherent reference wave, creating a high-contrast interference pattern. The interaction with the incoherent component merely added a homogeneous background, which was much less pronounced than the interference peaks. In the second experiment, the image and reference beams are combined at the monochromator without any additional spatial modulation. Thus each polariton state interferes with a delayed version of itself.

One should note that in the plane-wave interferometry experiment, vortex states do not manifest themselves on the interferogram because a vortex present in both the image and the reference beam does not introduce any additional phase shift between them. However, it is useful to acknowledge that detecting a vortex in plane waves is indeed possible [36]. This can be achieved by performing a mirror reflection of the reference beam in the plane of the section using a retroreflector.

Regarding the origin of azimuthal polariton currents, we are confident that the explanation proposed in our previous works [28–33] remains valid in the present scenario. As previously discussed, polariton currents in the trap were generated by a slight submicron radial displacement of the pump spot relative to the center of the micropillar. Such displacement alone does not break the equivalence between clockwise and counterclockwise directions. However, when combined with an additional symmetry-breaking factor, it can impart azimuthal chirality to the system, assigning a predominant direction of current flow. This factor could be, for instance, a local inhomogeneity in the stationary potential due to inevitable imperfections in the sample growth process or a slight modulation of the pump beam.

In our observations, the regions where polaritons predominantly accumulate in the experimentally observed condensate states are radially separated. Therefore, a suitably positioned local inhomogeneity that affects one state might have no impact on another due to the latter's low density in the relevant area. Consequently, for different radial sections of the trap, the predominant direction of the polariton current, induced by the displacement of the pump in conjunction with local potential landscape inhomogeneity, can vary.

A pair of polariton condensate states with azimuthal currents in arbitrary directions offers a promising foundation for developing a flux polariton qubit. The concept of such a qubit was initially proposed in a prior study [23], and recent efforts have been made toward its experimental realization using a superposition of current states in an annular optical trap [52]. The principle underlying the flux qubit involves leveraging the quantum superposition and entanglement of current states, which enables the encoding and manipulation of quantum information based on the directional flow of the currents. The concept of a polariton qubit utilizing dumbbell-like states in a trap has recently been developed theoretically [53] and experimentally [54].

A common approach in the cited works is to use a pair of condensate states as the qubit-forming states, that are characterized by the same radial quantum number and are degenerate in energy within an azimuthally symmetric trap. The splitting of these states is induced by an external perturbation of the effective potential. A distinctive feature

of the experimental geometry described by us is that the excited states inherently possess an energy splitting, which allows them to be utilized without additional preparation. The difference in the spatial distribution of the polariton densities serves as an additional factor that facilitates the precise identification and control of these states.

In the referenced studies, coherent coupling of the polariton states manifested as regular beats in PL intensity distribution, facilitated by splitting of the states in the trap on the order of tens of microelectronvolts. The splitting of the polariton condensate states we observed is estimated to be at least an order of magnitude larger, around 0.6 meV. In the current experiment, this splitting is sufficient to allow the condensates to evolve with a high degree of independence, without any detectable coherent influence on each other's phase properties. Such influence could manifest as additional dislocations in interference fringes [32,33] or as fluctuations in intensity contrast at varying phase delays in interferometric experiments. However, we observe no such effects.

The substantial splitting is maintained by the steep boundaries of the stationary potential of the cylindrical micropillar, in contrast to the more gradually varying boundaries of harmonic or other potlike potentials [44,54–57], where the effective trap width considerably varies across different eigenstates. The splitting magnitude can be adjusted by modifying the trap dimensions, such as the size of the pillar and the width of the ring trap, which is determined by the width of the central pumping spot. It is essential to ensure that the ring width remains sufficiently narrow to avoid broadening the spectrum excessively and to prevent the coexistence of waveguide modes with the spatially quantized modes of the trap [58]. Future research could explore the possibility of establishing coherent coupling between polariton current states with different radial quantum numbers to construct polariton-based flux qubits.

Another significant challenge for the possible practical realization of polariton flux qubits is maintaining coherence in polariton condensates. The primary sources of decoherence in these systems are the inherently nonequilibrium nature of polariton condensates due to the finite lifetime of polaritons, and their strong interactions with the incoherent exciton reservoir. To address the first issue, an effective approach is to increase the polariton lifetime by enhancing the quality factor of the microcavities through optimizing the number and uniformity of the Bragg reflector layers. Experimental studies [59–63] have demonstrated the possibility of achieving polariton lifetimes of several hundred picoseconds, which is at least an order of magnitude greater than one in our sample. As shown in Refs. [61–63], such extended lifetimes are sufficient to bring the polariton condensate to a thermal equilibrium, significantly reducing the effects of dissipation and enhancing coherence.

Regarding the second source of decoherence, the interaction with the exciton reservoir poses a more complex challenge because, while the incoherent exciton reservoir is a primary contributor to decoherence, it also serves as the source of replenishment for the condensate through nonresonant optical pumping. Thus, completely eliminating its influence is not feasible, but it can be significantly mitigated. An effective approach is to modify the size and geometry of the polariton trap. In the considered geometry, this involves using micropillars with larger diameters. When the size of the trap with a fixed geometry (ring shaped in our case) is changed, the set of its eigenstates remains consistent, while their absolute and relative positions on the energy scale shift. This alteration affects the interaction of these states with the external pumping, which is reflected, for example, in the change of the pump-power threshold. Of note, with an increase in the diameter of the micropillar, the overlap integral between the polariton state and the exciton reservoir, concentrated at the center of the pillar, decreases, thereby reducing the reservoir's contribution to decoherence. Such optimizations in microcavity design and trap configuration are essential steps towards achieving the coherence required for robust polariton-based quantum devices.

ACKNOWLEDGMENTS

V.L. and A.K. acknowledge Saint-Petersburg State University Research Project No. 122040800257-5. The work of V.L. was supported by the RSF Project No. 19-72-20039 (interferometry measurements). Numerical simulations were carried out within the state assignment in the field of scientific activity of the Ministry of Science and Higher Education of the Russian Federation (theme FZUN-2024-0019, state assignment of the VlSU).

[1] A. Kavokin, J. Baumberg, G. Malpuech, and F. Laussy, *Microcavities*, Series on Semiconductor Science and Technology (OUP Oxford, 2017), 2nd ed.

[2] J. Kasprzak, M. Richard, S. Kundermann, A. Baas, P. Jeambrun, J. M. J. Keeling, F. M. Marchetti, M. H. Szymańska, R. André, J. L. Staehli, V. Savona, P. B. Littlewood, B. Deveaud, and L. S. Dang, Bose–Einstein condensation of exciton polaritons, Nature **443**, 409 (2006).

[3] A. Metelmann and A. A. Clerk, Nonreciprocal photon transmission and amplification via reservoir engineering, Phys. Rev. X **5**, 021025 (2015).

[4] M. Keck, D. Rossini, and R. Fazio, Persistent currents by reservoir engineering, Phys. Rev. A **98**, 053812 (2018).

[5] M. Aßmann, F. Veit, M. Bayer, A. Löffler, S. Höfling, M. Kamp, and A. Forchel, All-optical control of quantized momenta on a polariton staircase, Phys. Rev. B **85**, 155320 (2012).

[6] N. Stroev and N. G. Berloff, Managing the flow of liquid light, Phys. Rev. B **102**, 201114 (2020).

[7] D. Sanvitto, F. M. Marchetti, M. H. Szymańska, G. Tosi, M. Baudisch, F. P. Laussy, D. N. Krizhanovskii, M. S. Skolnick, L. Marrucci, A. Lemaître, J. Bloch, C. Tejedor, and L. Viña, Persistent currents and quantized vortices in a polariton superfluid, Nat. Phys. **6**, 527 (2010).

[8] I. Carusotto and C. Ciuti, Quantum fluids of light, Rev. Mod. Phys. **85**, 299 (2013).

[9] A. V. Yulin, A. V. Nalitov, and I. A. Shelykh, Spinning polariton vortices with magnetic field, Phys. Rev. B **101**, 104308 (2020).

[10] K. G. Lagoudakis, M. Wouters, M. Richard, A. Baas, I. Carusotto, R. André, L. S. Dang, and B. Deveaud-Plédran, Quantized vortices in an exciton–polariton condensate, Nat. Phys. **4**, 706 (2008).

[11] F. Manni, T. C. H. Liew, K. G. Lagoudakis, C. Ouellet-Plamondon, R. André, V. Savona, and B. Deveaud, Spontaneous self-ordered states of vortex-antivortex pairs in a polariton condensate, Phys. Rev. B **88**, 201303 (2013).

[12] K. A. Sitnik, S. Alyatkin, J. D. Töpfer, I. Gnusov, T. Cookson, H. Sigurdsson, and P. G. Lagoudakis, Spontaneous formation of time-periodic vortex cluster in nonlinear fluids of light, Phys. Rev. Lett. **128**, 237402 (2022).

[13] D. N. Krizhanovskii, D. M. Whittaker, R. A. Bradley, K. Guda, D. Sarkar, D. Sanvitto, L. Vina, E. Cerda, P. Santos, K. Biermann, R. Hey, and M. S. Skolnick, Effect of interactions on vortices in a nonequilibrium polariton condensate, Phys. Rev. Lett. **104**, 126402 (2010).

[14] I. Gnusov, S. Harrison, S. Alyatkin, K. Sitnik, J. Töpfer, H. Sigurdsson, and P. Lagoudakis, Quantum vortex formation in the "rotating bucket" experiment with polariton condensates, Sci. Adv. **9**, eadd1299 (2023).

[15] Y. del Valle-Inclan Redondo, C. Schneider, S. Klembt, S. Höfling, S. Tarucha, and M. D. Fraser, Optically driven rotation of exciton–polariton condensates, Nano Lett. **23**, 4564 (2023).

[16] A. V. Yulin, I. A. Shelykh, E. S. Sedov, and A. V. Kavokin, Spin resonance induced by a mechanical rotation of a polariton condensate, Phys. Rev. B **108**, 045301 (2023).

[17] A. V. Yulin, I. A. Shelykh, E. S. Sedov, and A. V. Kavokin, Vorticity of polariton condensates in rotating traps, Phys. Rev. B **108**, 155301 (2023).

[18] A. V. Yulin, E. S. Sedov, A. V. Kavokin, and I. A. Shelykh, Persistent polarization oscillations in ring-shape polariton condensates, Phys. Rev. Res. **6**, 013261 (2024).

[19] M.-S. Kwon, B. Y. Oh, S.-H. Gong, J.-H. Kim, H. K. Kang, S. Kang, J. D. Song, H. Choi, and Y.-H. Cho, Direct transfer of light's orbital angular momentum onto a nonresonantly excited polariton superfluid, Phys. Rev. Lett. **122**, 045302 (2019).

[20] A. Mair, A. Vaziri, G. Weihs, and A. Zeilinger, Entanglement of the orbital angular momentum states of photons, Nature **412**, 313 (2001).

[21] A. Vaziri, G. Weihs, and A. Zeilinger, Experimental two-photon, three-dimensional entanglement for quantum communication, Phys. Rev. Lett. **89**, 240401 (2002).

[22] C. Perumangatt, N. Lal, A. Anwar, S. Gangi Reddy, and R. Singh, Quantum information with even and odd states of orbital angular momentum of light, Phys. Lett. A **381**, 1858 (2017).

[23] Y. Xue, I. Chestnov, E. Sedov, E. Kiktenko, A. K. Fedorov, S. Schumacher, X. Ma, and A. Kavokin, Split-ring polariton condensates as macroscopic two-level quantum systems, Phys. Rev. Res. **3**, 013099 (2021).

[24] A. Kavokin, T. C. H. Liew, C. Schneider, P. G. Lagoudakis, S. Klembt, and S. Hoefling, Polariton condensates for classical and quantum computing, Nat. Rev. Phys. **4**, 435 (2022).

[25] A. Askitopoulos, H. Ohadi, A. V. Kavokin, Z. Hatzopoulos, P. G. Savvidis, and P. G. Lagoudakis, Polariton condensation in an optically induced two-dimensional potential, Phys. Rev. B **88**, 041308 (2013).

[26] A. Askitopoulos, A. V. Nalitov, E. S. Sedov, L. Pickup, E. D. Cherotchenko, Z. Hatzopoulos, P. G. Savvidis, A. V. Kavokin, and P. G. Lagoudakis, All-optical quantum fluid spin beam splitter, Phys. Rev. B **97**, 235303 (2018).

[27] R. Dall, M. D. Fraser, A. S. Desyatnikov, G. Li, S. Brodbeck, M. Kamp, C. Schneider, S. Höfling, and E. A. Ostrovskaya, Creation of orbital angular momentum states with chiral polaritonic lenses, Phys. Rev. Lett. **113**, 200404 (2014).

[28] V. A. Lukoshkin, V. K. Kalevich, M. M. Afanasiev, K. V. Kavokin, Z. Hatzopoulos, P. G. Savvidis, E. S. Sedov, and A. V. Kavokin, Persistent circular currents of exciton-polaritons in cylindrical pillar microcavities, Phys. Rev. B **97**, 195149 (2018).

[29] E. Sedov, V. Lukoshkin, V. Kalevich, Z. Hatzopoulos, P. Savvidis, and A. Kavokin, Persistent currents in half-moon polariton condensates, ACS Photonics **7**, 1163 (2020).

[30] E. S. Sedov, V. A. Lukoshkin, V. K. Kalevich, P. G. Savvidis, and A. V. Kavokin, Circular polariton currents with integer and fractional orbital angular momenta, Phys. Rev. Res. **3**, 013072 (2021).

[31] E. S. Sedov, V. A. Lukoshkin, V. K. Kalevich, I. Y. Chestnov, Z. Hatzopoulos, P. G. Savvidis, and A. V. Kavokin, Double ring polariton condensates with polariton vortices, Nanosystems: Phys. Chem. Math. **13**, 608 (2022).

[32] V. Lukoshkin, E. Sedov, V. Kalevich, Z. Hatzopoulos, P. G. Savvidis, and A. Kavokin, Steady state oscillations of circular currents in concentric polariton condensates, Sci. Rep. **13**, 4607 (2023).

[33] V. A. Lukoshkin, I. E. Sedova, V. K. Kalevich, E. S. Sedov, Z. Hatzopoulos, P. G. Savvidis, and A. V. Kavokin, Oscillating vorticity in single ring exciton polariton condensates, Nanosystems: Phys. Chem. Math. **14**, 328 (2023).

[34] E. Sedov, S. Arakelian, and A. Kavokin, Spontaneous symmetry breaking in persistent currents of spinor polaritons, Sci. Rep. **11**, 22382 (2021).

[35] J. Barrat, R. Cherbunin, E. Sedov, E. Aladinskaia, A. Liubomirov, V. Litvyak, M. Petrov, X. Zhou, Z. Hatzopoulos, A. Kavokin, and P. G. Savvidis, Stochastic circular persistent currents of exciton polaritons, Sci. Rep. **14**, 12953 (2024).

[36] Q. Yao, P. Comaron, H. A. Alnatah, J. Beaumariage, S. Mukherjee, K. West, L. Pfeiffer, K. Baldwin, M. Szymańska, and D. W. Snoke, Persistent, controllable circulation of a polariton ring condensate, arXiv:2302.07803 [cond-mat.quant-gas].

[37] V. G. Sala, D. D. Solnyshkov, I. Carusotto, T. Jacqmin, A. Lemaître, H. Terças, A. Nalitov, M. Abbarchi, E. Galopin, I. Sagnes, J. Bloch, G. Malpuech, and A. Amo, Spin-orbit coupling for photons and polaritons in microstructures, Phys. Rev. X **5**, 011034 (2015).

[38] K. G. Lagoudakis, B. Pietka, M. Wouters, R. André, and B. Deveaud-Plédran, Coherent oscillations in an exciton-polariton Josephson junction, Phys. Rev. Lett. **105**, 120403 (2010).

[39] N. Voronova, A. Grudinina, R. Panico, D. Trypogeorgos, M. D. Giorgi, K. Baldwin, L. Pfeiffer, D. Sanvitto, and D. Ballarini, Exciton-polariton ring Josephson junction, arXiv:2404.12663 [cond-mat.mes-hall].

[40] A. Muñoz Mateo, Y. G. Rubo, and L. A. Toikka, Long Josephson junctions with exciton-polariton condensates, Phys. Rev. B **101**, 184509 (2020).

[41] I. Chestnov, A. Yulin, I. A. Shelykh, and A. Kavokin, Dissipative Josephson vortices in annular polariton fluids, Phys. Rev. B **104**, 165305 (2021).

[42] V. K. Kalevich, M. M. Afanasiev, V. A. Lukoshkin, D. D. Solnyshkov, G. Malpuech, K. V. Kavokin, S. I. Tsintzos, Z. Hatzopoulos, P. G. Savvidis, and A. V. Kavokin, Controllable structuring of exciton-polariton condensates in cylindrical pillar microcavities, Phys. Rev. B **91**, 045305 (2015).

[43] A. V. Nalitov, H. Sigurdsson, S. Morina, Y. S. Krivosenko, I. V. Iorsh, Y. G. Rubo, A. V. Kavokin, and I. A. Shelykh, Optically trapped polariton condensates as semiclassical time crystals, Phys. Rev. A **99**, 033830 (2019).

[44] E. Aladinskaia, R. Cherbunin, E. Sedov, A. Liubomirov, K. Kavokin, E. Khramtsov, M. Petrov, P. G. Savvidis, and A. Kavokin, Spatial quantization of exciton-polariton condensates in optically induced traps, Phys. Rev. B **107**, 045302 (2023).

[45] P. Tsotsis, P. S. Eldridge, T. Gao, S. I. Tsintzos, Z. Hatzopoulos, and P. G. Savvidis, Lasing threshold doubling at the crossover from strong to weak coupling regime in GaAs microcavity, New J. Phys. **14**, 023060 (2012).

[46] F. Barkhausen, M. Pukrop, S. Schumacher, and X. Ma, Structuring coflowing and counterflowing currents of polariton condensates in concentric ring-shaped and elliptical potentials, Phys. Rev. B **103**, 075305 (2021).

[47] J. Beierlein, E. Rozas, O. A. Egorov, M. Klaas, A. Yulin, H. Suchomel, T. H. Harder, M. Emmerling, M. D. Martín, I. A. Shelykh, C. Schneider, U. Peschel, L. Viña, S. Höfling, and S. Klembt, Propagative oscillations in codirectional polariton waveguide couplers, Phys. Rev. Lett. **126**, 075302 (2021).

[48] I. Sedova and E. Sedov, Polarization conversion in a polariton three-waveguide coupler, Results in Optics **4**, 100105 (2021).

[49] D. Schmidt, B. Berger, M. Kahlert, M. Bayer, C. Schneider, S. Höfling, E. S. Sedov, A. V. Kavokin, and M. Aßmann, Tracking dark excitons with exciton polaritons in semiconductor microcavities, Phys. Rev. Lett. **122**, 047403 (2019).

[50] E. Rozas, E. Sedov, Y. Brune, S. Höfling, A. Kavokin, and M. Aßmann, Polariton–dark exciton interactions in bistable semiconductor microcavities, Phys. Rev. B **108**, 165411 (2023).

[51] The effective mass of polaritons is $M = 5 \times 10^{-5} m_e$, where m_e is the free electron mass. The energy difference of the modes is $\delta\varepsilon = 0.6$ meV. The polariton and reservoir exciton decay rates are taken as $\gamma_1 = 0.02$ ps^{-1}, $\gamma_2 = 0.021$ ps^{-1}, and $\gamma_R = 0.025$ ps^{-1}, respectively. The stimulated scattering rates are taken as $\hbar R_1 = 0.04$ meV μm^2 and $\hbar R_2 = 0.05$ meV μm^2. The nonlinearity coefficients are taken as $\alpha = 1.1\alpha_{12} = \alpha_R/2 = 3$ μeV μm^2. The energy relaxation is $\eta_0 = 0.1$. The pump repulsion coefficient is $G = 1.5$ μeV s μm^2. The widths characterizing the pump are $w = 4.5$ μm and $\bar{w} = 3$ μm. The parameters of the stationary potential are $d = 30$ μm and $d' = 30.8$ μm, $V_0 = 40$ μeV and $\bar{V}_0 = 3$ μeV.

[52] J. Barrat, A. F. Tzortzakakis, M. Niu, X. Zhou, G. G. Paschos, D. Petrosyan, and P. G. Savvidis, Qubit analog with polariton superfluid in an annular trap, Sci. Adv. **10**, eado4042 (2024).

[53] L. S. Ricco, I. A. Shelykh, and A. Kavokin, Qubit gate operations in elliptically trapped polariton condensates, Sci. Rep. **14**, 4211 (2024).

[54] R. V. Cherbunin, A. Liubomirov, D. Novokreschenov, A. Kudlis, and A. V. Kavokin, Quantum beats of a macroscopic polariton condensate in real space, arXiv:2407.12429 [cond-mat.mes-hall].

[55] M. Pieczarka, M. Boozarjmehr, E. Estrecho, Y. Yoon, M. Steger, K. West, L. N. Pfeiffer, K. A. Nelson, D. W. Snoke, A. G. Truscott, and E. A. Ostrovskaya, Effect of optically induced potential on the energy of trapped exciton polaritons below the condensation threshold, Phys. Rev. B **100**, 085301 (2019).

[56] E. S. Sedov, Y. G. Rubo, and A. V. Kavokin, Polariton polarization rectifier, Light: Science & Applications **8**, 79 (2019).

[57] E. Sedov, I. Sedova, S. Arakelian, and A. Kavokin, Polygonal patterns of confined light, Opt. Lett. **46**, 1836 (2021).

[58] Q. Yao, E. Sedov, S. Mukherjee, J. Beaumariage, B. Ozden, K. West, L. Pfeiffer, A. Kavokin, and D. W. Snoke, Ballistic transport of a polariton ring condensate with spin precession, Phys. Rev. B **106**, 245309 (2022).

[59] B. Nelsen, G. Liu, M. Steger, D. W. Snoke, R. Balili, K. West, and L. Pfeiffer, Dissipationless flow and sharp threshold of a polariton condensate with long lifetime, Phys. Rev. X **3**, 041015 (2013).

[60] D. M. Myers, B. Ozden, M. Steger, E. Sedov, A. Kavokin, K. West, L. N. Pfeiffer, and D. W. Snoke, Superlinear increase of photocurrent due to stimulated scattering into a polariton condensate, Phys. Rev. B **98**, 045301 (2018).

[61] Y. Sun, P. Wen, Y. Yoon, G. Liu, M. Steger, L. N. Pfeiffer, K. West, D. W. Snoke, and K. A. Nelson, Bose-Einstein condensation of long-lifetime polaritons in thermal equilibrium, Phys. Rev. Lett. **118**, 016602 (2017).

[62] H. Alnatah, Q. Yao, J. Beaumariage, S. Mukherjee, M. C. Tam, Z. Wasilewski, K. West, K. Baldwin, L. N. Pfeiffer, and D. W. Snoke, Coherence measurements of polaritons in thermal equilibrium reveal a power law for two-dimensional condensates, Sci. Adv. **10**, eadk6960 (2024).

[63] D. Caputo, D. Ballarini, G. Dagvadorj, C. Sánchez Muñoz, M. De Giorgi, L. Dominici, K. West, L. N. Pfeiffer, G. Gigli, F. P. Laussy, M. H. Szymańska, and D. Sanvitto, Topological order and thermal equilibrium in polariton condensates, Nat. Mater. **17**, 145 (2018).